LETTER

doi:10.1038/nature13081

Structure of a type IV secretion system

Harry H. Low[1]*†, Francesca Gubellini[2]*, Angel Rivera-Calzada[1], Nathalie Braun[1], Sarah Connery[1], Annick Dujeancourt[2], Fang Lu[1], Adam Redzej[1], Rémi Fronzes[2], Elena V. Orlova[1] & Gabriel Waksman[1]

Bacterial type IV secretion systems translocate virulence factors into eukaryotic cells[1,2], distribute genetic material between bacteria and have shown potential as a tool for the genetic modification of human cells[3]. Given the complex choreography of the substrate through the secretion apparatus[4], the molecular mechanism of the type IV secretion system has proved difficult to dissect in the absence of structural data for the entire machinery. Here we use electron microscopy to reconstruct the type IV secretion system encoded by the *Escherichia coli* R388 conjugative plasmid. We show that eight proteins assemble in an intricate stoichiometric relationship to form an approximately 3 megadalton nanomachine that spans the entire cell envelope. The structure comprises an outer membrane-associated core complex[1] connected by a central stalk to a substantial inner membrane complex that is dominated by a battery of 12 VirB4 ATPase subunits organized as side-by-side hexameric barrels. Our results show a secretion system with markedly different architecture, and consequently mechanism, to other known bacterial secretion systems[1,4–6].

The canonical type IV secretion (T4S) system comprises 12 proteins, VirB1–11 and VirD4, and forms a large macromolecular complex that spans the cell envelope of Gram-negative bacteria[2]. The hub protein VirB10 inserts into both the inner and outer membranes and spans the entire width of the periplasm. It is decorated by VirB7 and VirB9 in a 1:1:1 ratio to form a C_{14} symmetrized outer membrane pore termed the core complex[7]. The architecture and relative topological positioning of the rest of the T4S system components, particularly at the inner membrane, are unknown. Three ATPases, VirB4, VirB11 and VirD4, energize the secretion apparatus[1,2,8]. Some T4S systems are known to extend a substantial tubular pilus, comprising VirB2 supplemented with a minor component, VirB5, beyond the cell boundary[1,2].

To provide structural insights into an assembled T4S system, the *virB/trw* operon of the R388 plasmid from *virB1/trwN* to *virB10/trwE* ($T4SS_{1-10}$) was cloned, overexpressed in *E. coli* and the solubilized membrane fraction subjected to affinity chromatography (Extended Data Fig. 1a). Analysis of eluted sample by SDS–polyacrylamide gel electrophoresis (SDS–PAGE) (Fig. 1a), liquid chromatography mass spectrometry (LC–MS) and western blot (Extended Data Fig. 1b) reproducibly showed a purified complex consisting of VirB3/TrwM, VirB4/TrwK, VirB5/TrwJ, VirB6/TrwI, VirB7/TrwH, VirB8/TrwG, VirB9/TrwF and VirB10/TrwE (termed the $T4SS_{3-10}$ complex). Overexpression of *virB1/trwN* to *virB11/trwD* with *virB10/trwE* tagged as in the $T4SS_{1-10}$ clone yielded the same $T4SS_{3-10}$ complex.

To characterize the three-dimensional architecture of the $T4SS_{3-10}$ complex, a negative-stain electron microscopy data set was collected. Characteristic views of the complex (class averages) were obtained that typically showed double barrel-like densities connected by a thin central stalk to a structure clearly reminiscent of the pKM101 plasmid core complex[7] (Fig. 1b). Indeed, separate purification of R388 VirB7/TrwH, VirB9/TrwF and VirB10/TrwE, and negative-stain electron microscopy of the resultant complex, confirmed formation of a pKM101-like core complex complete with 14-fold symmetry (Extended Data Fig. 2). In the $T4SS_{3-10}$ assembly, those densities outside the obvious core complex are broadly termed the inner membrane complex (IMC) (Fig. 1b). Significant flexibility between IMC and the core complex was observed (Extended Data Fig. 3a–c), which prompted two discrete three-dimensional reconstructions to be generated for the two complexes (Extended Data Fig. 3d). Final resolutions of 18 Å and 23 Å were achieved, respectively (Extended Data Fig. 4a), with flexibility in the IMC accounting for the difference in resolutions. Ultimately, these reconstructions were merged

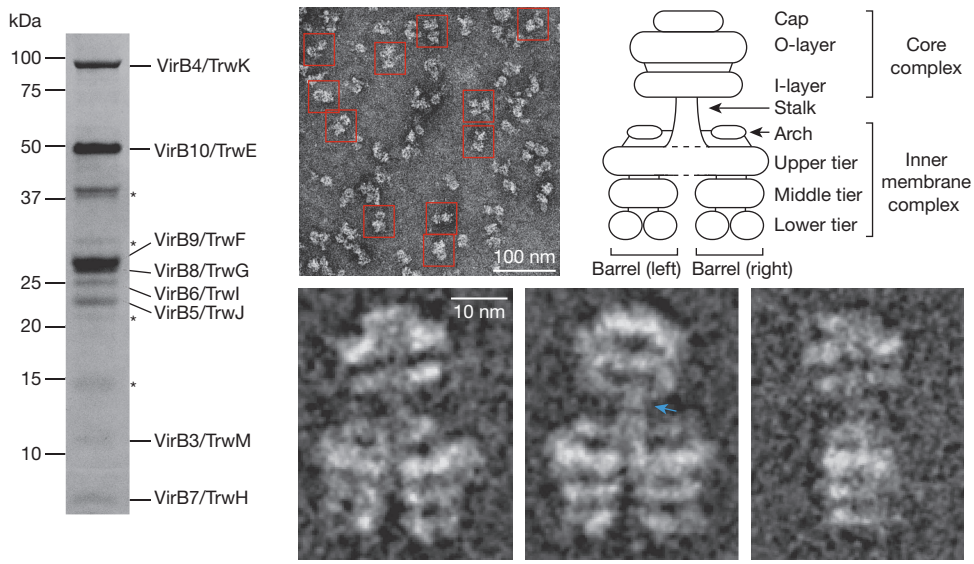

Figure 1 | Purification of the R388 encoded $T4SS_{3-10}$ complex. a, SDS–PAGE of the $T4SS_{3-10}$ complex. Asterisks indicate minor contaminants (from top to bottom: OmpF/OmpA, dihydrolipoyl dehydrogenase, single-stranded DNA-binding protein and lysozyme). **b**, Overview negative-stain electron microscope image and representative characteristic views (class averages) of the $T4SS_{3-10}$ complex with a schematic describing the nomenclature of observed structure components. Blue arrow indicates region of high flexibility.

[1]Institute of Structural and Molecular Biology, University College London and Birkbeck College, Malet Street, London WC1E 7HX, UK. [2]Institut Pasteur, G5 Biologie structurale de la sécrétion bactérienne and UMR 3528-CNRS, 25 rue du Docteur Roux, 75015 Paris, France. †Present address: Faculty of Natural Sciences, Imperial College, London SW7 2AZ, UK.
*These authors contributed equally to this work.

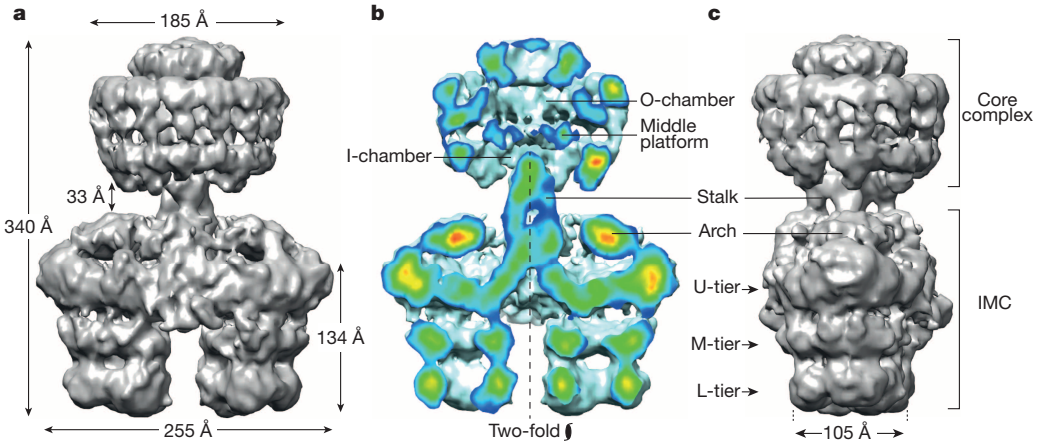

Figure 2 | Asymmetric composite structure of the T4SS$_{3-10}$ complex. **a**, Front view. The map is a composite generated by merging independently processed core complex and IMC reconstructions. **b**, Cut-away front view. Electron density is colour-coded, ranging from red to blue, indicating regions of strong to weak density, respectively. The IMC has pseudo-two-fold symmetry around the particle long axis. **c**, Side view. U-, M- and L-tier substitute for upper, middle and lower tier, respectively.

to generate a composite map of the entire T4SS$_{3-10}$ complex (Figs 2 and 3a and Extended Data Fig. 4b–e). Final maps were generated with no symmetry applied. However, C_{14} symmetry is clearly observed in the core complex and overall C_2 symmetry in the IMC (Fig. 2).

The whole T4SS$_{3-10}$ complex is 340 Å in length and comprises a core complex connected by a central stalk to an IMC that is 255 Å at its widest (Fig. 2). The observed core complex is similar to that of the well-characterized pKM101 plasmid[7,9], with a diameter of 185 Å and rotationally symmetric inner (I-) and outer (O-) layers integrated to form a chamber that is divided by a central middle platform (Fig. 3b). The core complex cap is in an overall closed conformation as in the cryo-electron microscopy reconstruction of the pKM101 core complex[9], with any central constriction[7] probably occluded by the negative stain of bound detergent or lipid, or both.

In contrast to previous T4S system core-complex reconstructions[7,9,10], the inner (I-) chamber is partly occluded by the central stalk (Fig. 3b–d), which extends distally from the core complex to form a central binding hub within the IMC. The stalk does not show any clear symmetry, and in the composite T4SS$_{3-10}$ complex model it makes several limited contacts with the walls of the I-chamber. The top and middle parts of the stalk are linked by four connections that varied in intensity during refinement, with the central pair being most stable (Fig. 3c and Extended Data Fig. 5a). Other connections may exist that were not observed owing to marked flexibility in this region (Extended Data Fig. 3b, c).

Connected to the stalk distal end are two barrel-like densities related by C_2 symmetry with length 134 Å and minimum diameter 105 Å (Fig. 2). Each barrel comprises three tiers, with the lower and middle tiers constituting rings with three-fold symmetry oriented around a central channel. In addition, a dimeric arrangement of densities around each three-fold axis is observed in the middle tier (Fig. 3e). The upper tier is more substantial and any central channel appears closed. Overall, each barrel comprises three basic elongated segments that are each made up of two subunits (Extended Data Fig. 5b).

Directly above the upper tier of each barrel lies a remarkable structure termed the arch, which interconnects between barrel subunits and the central stalk (Figs 2 and 3d). Each arch comprises a substantial central density that contacts the underlying barrel through up to six thin linkers (Extended Data Fig. 5a). Note that not all linkers were consistently resolved during refinement and often only a dominant triad of links was observed (positions 1, 3 and 5 in Extended Data Fig. 5a).

To ensure that dry preparation of samples did not affect the integrity of the particles, a tilt series experiment using cryo-negative-stain electron microscopy was performed. It confirmed the features and dimensions of the T4SS$_{3-10}$ complex reconstruction described above (Extended Data Fig. 6).

To begin dissecting the internal organization of the T4SS$_{3-10}$ complex, the stoichiometry of its constituents was determined using radioiodination[11]. A T4SS$_{3-10}$ complex clone variant was used in which a

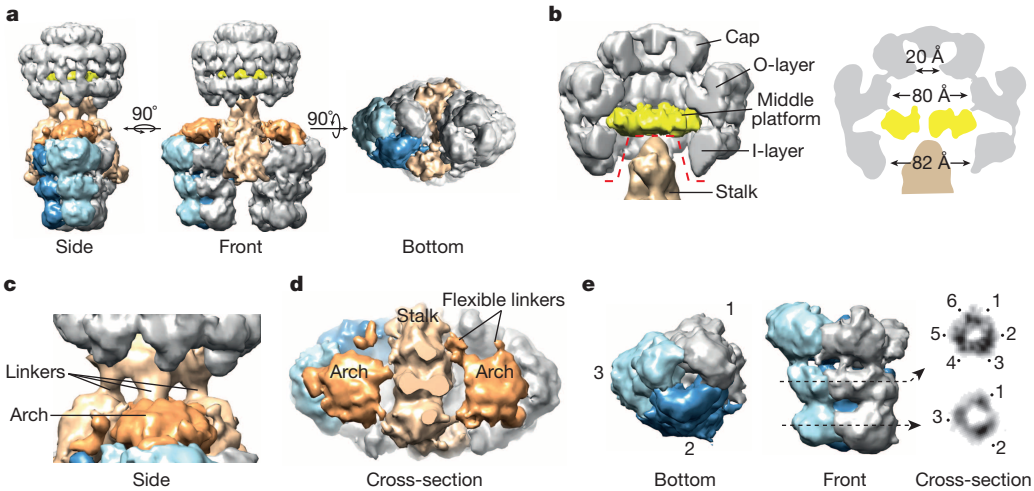

Figure 3 | Segmentation of the T4SS$_{3-10}$ complex reconstruction. **a**, Side, front and bottom views. Of the two barrels, only the left one is segmented. The colour scheme used is upheld in all panels. **b**, Zoom cut-away view of the core complex and stalk. Dashed red line delineates the border at which the separate core complex and IMC reconstructions were merged (left). Central cross-section schematic of the core complex from this study (right). **c**, Zoom side view of the stalk. Some of the linkers between the core complex and IMC are flexible and were therefore poorly resolved. **d**, Cut-away top view of the stalk and arches. **e**, Each barrel-like density consists of three dimeric elongated segments. Cross-sections of the lower and middle tiers (right panel) show three-fold symmetry with a trimer of dimeric densities present in the middle tier.

His-tag was incorporated at the amino (N) terminus of VirB6/TrwI ($T4SS_{3-10/His6\text{-}B6}$). The $T4SS_{3-10/His6\text{-}B6}$ complex showed improved biochemical stability and was equivalent to the $T4SS_{3-10}$ complex when analysed by electron microscopy (Extended Data Fig. 7a). Using the known 14-fold copy number of VirB10/TrwE[7,12] for calibration, the relative stoichiometry of VirB4/TrwK, VirB6/TrwI and VirB5/TrwJ is 11.5:23.8:11.9 (Fig. 4a). Deconvolution of overlapping iodine-125 signals for VirB9/TrwF and VirB8/TrwG, based on a copy number of 14 for VirB9/TrwF[7,12], suggests there are 12.6 copies of VirB8/TrwG (Fig. 4a). VirB7/TrwH has no tyrosine residue but its stoichiometry within the core complex is known and is the same as VirB10/TrwE. As radio-iodination was unsuitable for VirB3/TrwM owing to a low iodine-125 signal, VirB4/TrwK and VirB3/TrwM were co-expressed independently and purified as a distinct complex from the membrane fraction. Gel filtration and SDS–PAGE showed that these proteins co-elute (Fig. 4b and Extended Data Fig. 7b). Quantification of the respective bands showed a stoichiometry of 1:1 (Fig. 4b). Strikingly, it therefore seems that all constituents of the $T4SS_{3-10}$ complex, excluding those of the core complex, essentially exist in multiples of 12. The combined stoichiometry data suggest the $T4SS_{3-10}$ complex is approximately 3.4 MDa, which correlates well with the calculated mass estimation derived from the map volume (~3.0 MDa).

The stacked three-tier architecture of the IMC barrels is reminiscent of the hexameric electron microscopy reconstruction of VirB4/TrwK[13]. Indeed, gold labelling of the $T4SS_{3-10}$ complex with a His-tag incorporated at the carboxy (C) terminus of VirB4/TrwK ($T4SS_{3-10/\ B4\text{-}His6}$) shows localization of label to both IMC barrels (Fig. 4c and Extended Data Fig. 8a, c). Negative-stain electron microscopy of VirB4/TrwK purified from the membrane fraction or as an N-terminal maltose-binding protein (MBP) fusion shows an elongated and flexible monomer with approximate length 105 Å (Extended Data Fig. 7c–e), which is consistent with the internal length of an IMC barrel. Such data, combined with the VirB4/TrwK stoichiometry and the observed trimer of dimer symmetry within each IMC barrel, support a model in which each barrel contains six VirB4/TrwK monomers. Gold labelling of VirB6/TrwI ($T4SS_{3-10/His6\text{-}B6}$ complex) shows a similar localization pattern to that of VirB4/TrwK, which suggests the VirB4/TrwK C terminus and VirB6/TrwI N terminus are in the same region within the complex (Fig. 4d and Extended Data Fig. 8b, c).

To deduce the position of the inner membrane, the relationship between VirB4/TrwK and the inner membrane was investigated. During $T4SS_{3-10/B4\text{-}His6}$ complex purification, sequential washing of the membrane fraction with 6 M urea, high pH and high salt solutions failed to separate VirB4/TrwK (Extended Data Fig. 7f), which suggests robust insertion of VirB4/TrwK within the inner membrane. Incorporating data from previous studies[13,14], it is proposed that the lower and middle tiers of each VirB4/TrwK barrel house the cytoplasmic VirB4/TrwK C terminus, whereas the upper tier is either partly or wholly inserted within the inner membrane and houses the VirB4/TrwK N terminus. Importantly, the soluble VirB4 C-terminal ATPase domain from

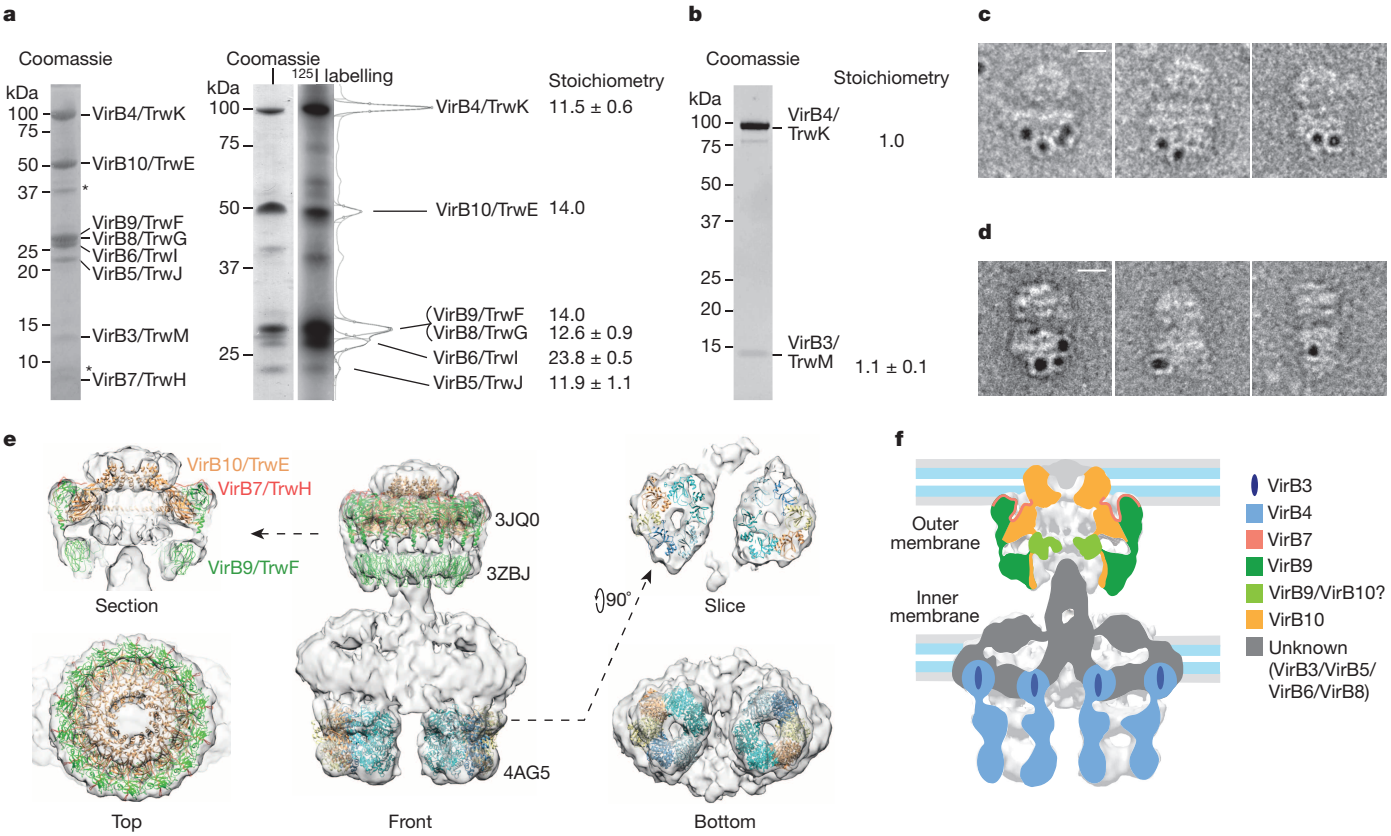

Figure 4 | Stoichiometric analysis and localization of various macromolecular components within the $T4SS_{3-10}$ complex reconstruction. **a**, Iodine-125 labelling of $T4SS_{3-10/His6\text{-}B6}$ complex constituent proteins. Left, SDS–PAGE of the $T4SS_{3-10/His6\text{-}B6}$ complex. * indicates minor contaminants (OmpF/OmpA and Lpp). Right, SDS–PAGE of ^{125}I-labelled proteins in left lane (Coomassie) and corresponding radiograph in right lane (iodine-125 labelling). Relative stoichiometry was calculated by integration of band intensity and is shown at right. Reported means and corresponding standard deviations are from two separate labelling experiments on four independent purifications. **b**, SDS–PAGE of the VirB4/TrwK and VirB3/TrwM complex stained with SYPRO Ruby. Relative stoichiometry was calculated by integration of band intensity and is shown at right. Reported means and corresponding standard deviations are from two independent purifications. **c**, Gold labelling (5 nm) of VirB4/TrwK clusters around the IMC barrels. Scale bar, 10 nm. **d**, Gold labelling (5 nm) of VirB6/TrwI shows a similar localization pattern to that of VirB4/TrwK (see **c**). Scale bar, 10 nm. **e**, Fit of the VirB4 ATPase domain from *T. pseudethanolicus* (4AG5), the pKM101 outer membrane complex (3JQ0) and the *in silico* model of VirB9/TraO (3ZBJ). **f**, Summary schematic showing the localization of known components and position of cell membranes. For clarity, only VirB nomenclature is used in the colour key.

Thermoanaerobacter pseudethanolicus fits optimally as a trimer of dimer arrangement within the lower and middle tiers (Fig. 4e)[10].

The compelling fit of the pKM101 outer membrane complex structure[12] and *in silico* VirB9/TraO I-layer model[9] into the core complex of the $T4SS_{3-10}$ reconstruction (Fig. 4e) highlights the unexpected distance (~40 Å) between the I-layer base and the proposed position of the inner membrane (Fig. 4f). The VirB10/TrwE N termini, extending distally from the base of the I-layer, either as part of the stalk or as distinct strands, must span this space to insert into the inner membrane (Extended Data Fig. 9a). This architecture suggests that substrate could also access the core complex secretion chamber from within the periplasm. Such a model is compatible with some T4S systems thought to use a two-step process[15,16]. Substrate would first cross the inner membrane using either the VirD4/TrwB coupling protein, VirB4/TrwK, or the Sec machinery in some other T4S systems. Then, secondarily, substrate would be channelled into the core complex and extruded (Extended Data Fig. 9b). Evidence is also mounting for interaction between VirD4/TrwB, VirB4/TrwK and VirB11/TrwD[17]. VirB4/TrwK hexamers could recruit, or even be replaced by, VirB11/TrwD or VirD4/TrwB, which would allow different enzymatic and functional gearing of the T4S machinery during the secretion cycle.

When compared with the type III secretion (T3S) system[18] (the only known structure for an assembled secretion system; Extended Data Fig. 10), the T4S system shows a fundamentally different architecture. While T3S systems are organized as a series of integrated ring-like structures that form a continuous tubular conduit, T4S systems show a more modular design with a two-fold symmetric inner-membrane complex conjoined by a central stalk to a concentric outer membrane channel. Thus T4S systems represent a radically different evolutionary approach, design and mechanism for the translocation of substrate across the bacterial cell envelope.

METHODS SUMMARY

The region from *virB1/trwN* to *virB10/trwE* ($T4SS_{1-10}$) was cloned from the *E. coli* R388 plasmid into pASK3c and pBAD vectors with a StrepII tag encoding sequence at the 3′ terminus of *virB10/trwE*. Constructs $T4SS_{1-10/B4\text{-}His6}$ and $T4SS_{1-10/His6\text{-}B6}$ derived from pBAD:$T4SS_{1-10}$ had His6-tags inserted at the C and N termini of VirB4/TrwK and VirB6/TrwI, respectively. The pASK3c:$T4SS_{3-4}$ construct was used to express the VirB3/TrwM–VirB4/TrwK complex. The $T4SS_{3-10}$ complex was extracted from bacterial membranes by mild solubilization using a detergent mixture of 0.5% w/v *n*-dodecyl-β-D-maltopyranoside (DDM), 0.75% w/v Decyl Maltose Neopentyl Glycol (DM-NPG) and 0.1% w/v digitonin, and purified by the StrepII tag. Gold labelling of the $T4SS_{3-10/B4\text{-}His6}$ and $T4SS_{3-10/His6\text{-}B6}$ complexes used 5 nm diameter Ni-NTA nanogold beads. Stoichiometry was determined by iodine-125 incorporation in tyrosine residues using purified $T4SS_{3-10/His6\text{-}B6}$. Samples were stained with uranyl acetate for negative-stain electron microscopy, or ammonium molybdate for cryo-negative-stain electron microscopy, on carbon-coated copper grids. Grids were examined using mostly a Tecnai F20 FEG microscope operating at a voltage of 200 kV. Images were recorded on a Gatan UltraScan 4000 CCD camera. For the $T4SS_{3-10}$ complex, a total of 21,680 particles were selected manually using BOXER[19]. Contrast transfer function (CTF) was estimated and corrected using CTFFIND3 (ref. 20) and BSOFT[21], respectively. Particle alignment steps, multivariate statistical analysis (MSA)[22], angular reconstitution, three-dimensional reconstruction and structure refinement were performed using IMAGIC[23] and SPIDER[24]. The core complex/stalk and IMC regions were then separately processed to generate two discrete maps. The two map densities were adjusted to equivalent standard deviation and then overlaid using the core complex I-layer as reference for superimposition.

Online Content Any additional Methods, Extended Data display items and Source Data are available in the online version of the paper; references unique to these sections appear only in the online paper.

Received 24 September 2013; accepted 27 January 2014.
Published online 9 March 2014.

1. Fronzes, R., Christie, P. J. & Waksman, G. The structural biology of type IV secretion systems. *Nature Rev. Microbiol.* **7,** 703–714 (2009).
2. Schröder, G. & Lanka, E. The mating pair formation system of conjugative plasmids—a versatile secretion machinery for transfer of proteins and DNA. *Plasmid* **54,** 1–25 (2005).
3. Schröder, G., Schuelein, R., Quebatte, M. & Dehio, C. Conjugative DNA transfer into human cells by the VirB/VirD4 type IV secretion system of the bacterial pathogen *Bartonella henselae*. *Proc. Natl Acad. Sci. USA* **108,** 14643–14648 (2011).
4. Cascales, E. & Christie, P. J. Definition of a bacterial type IV secretion pathway for a DNA substrate. *Science* **304,** 1170–1173 (2004).
5. Johnson, T. L., Abendroth, J., Hol, W. G. & Sandkvist, M. Type II secretion: from structure to function. *FEMS Microbiol. Lett.* **255,** 175–186 (2006).
6. Marlovits, T. C. *et al.* Structural insights into the assembly of the type III secretion needle complex. *Science* **306,** 1040–1042 (2004).
7. Fronzes, R. *et al.* Structure of a type IV secretion system core complex. *Science* **323,** 266–268 (2009).
8. Kerr, J. E. & Christie, P. J. Evidence for VirB4-mediated dislocation of membrane-integrated VirB2 pilin during biogenesis of the *Agrobacterium* VirB/VirD4 type IV secretion system. *J. Bacteriol.* **192,** 4923–4934 (2010).
9. Rivera-Calzada, A. *et al.* Structure of a bacterial type IV secretion core complex at subnanometre resolution. *EMBO J.* **32,** 1195–1204 (2013).
10. Wallden, K. *et al.* Structure of the VirB4 ATPase, alone and bound to the core complex of a type IV secretion system. *Proc. Natl Acad. Sci. USA* **109,** 11348–11353 (2012).
11. Passmore, L. A. *et al.* Structural analysis of the anaphase-promoting complex reveals multiple active sites and insights into polyubiquitylation. *Mol. Cell* **20,** 855–866 (2005).
12. Chandran, V. *et al.* Structure of the outer membrane complex of a type IV secretion system. *Nature* **462,** 1011–1015 (2009).
13. Peña, A. *et al.* The hexameric structure of a conjugative VirB4 protein ATPase provides new insights for a functional and phylogenetic relationship with DNA translocases. *J. Biol. Chem.* **287,** 29925–29932 (2012).
14. Durand, E., Oomen, C. & Waksman, G. Biochemical dissection of the ATPase TraB, the VirB4 homologue of the *Escherichia coli* pKM101 conjugation machinery. *J. Bacteriol.* **192,** 2315–2323 (2010).
15. Locht, C., Coutte, L. & Mielcarek, N. The ins and outs of pertussis toxin. *FEBS J.* **278,** 4668–4682 (2011).
16. Pantoja, M., Chen, L. S., Chen, Y. C. & Nester, E. W. *Agrobacterium* type IV secretion is a two-step process in which export substrates associate with the virulence protein VirJ in the periplasm. *Mol. Microbiol.* **45,** 1325–1335 (2002).
17. Ripoll-Rozada, J., Zunzunegui, S., de la Cruz, F., Arechaga, I. & Cabezon, E. Functional interactions of VirB11 traffic ATPases with VirB4 and VirD4 molecular motors in type IV secretion systems. *J. Bacteriol.* **195,** 4195–4201 (2013).
18. Schraidt, O. & Marlovits, T. C. Three-dimensional model of *Salmonella*'s needle complex at subnanometer resolution. *Science* **331,** 1192–1195 (2011).
19. Ludtke, S. J., Baldwin, P. R. & Chiu, W. EMAN: Semiautomated software for high-resolution single-particle reconstructions. *J. Struct. Biol.* **128,** 82–97 (1999).
20. Mindell, J. A. & Grigorieff, N. Accurate determination of local defocus and specimen tilt in electron microscopy. *J. Struct. Biol.* **142,** 334–347 (2003).
21. Heymann, J. B. Bsoft: Image and molecular processing in electron microscopy. *J. Struct. Biol.* **133,** 156–169 (2001).
22. van Heel, M. *et al.* Single-particle electron cryo-microscopy: towards atomic resolution. *Q. Rev. Biophys.* **33,** 307–369 (2000).
23. vanHeel, M., Harauz, G., Orlova, E. V., Schmidt, R. & Schatz, M. A new generation of the IMAGIC image processing system. *J. Struct. Biol.* **116,** 17–24 (1996).
24. Frank, J. *et al.* SPIDER and WEB: processing and visualization of images in 3D electron microscopy and related fields. *J. Struct. Biol.* **116,** 190–199 (1996).

Acknowledgements This work was financed by grant 098302 from the Wellcome Trust to G.W. and by equipment grant 079605 from the Wellcome Trust. R.F. and A.D. were financed by Institut Pasteur and the CNRS. F.G. was the recipient of 'Bourse Roux' from Institut Pasteur. We thank G. Péhau-Arnaudet for support with the electron microscopes at Institut Pasteur.

Author Contributions H.H.L., F.G., R.F., E.V.O. and G.W. designed the experiments. H.H.L., F.G., S.C. and F.L. generated the clones. H.H.L. first purified the $T4SS_{3-10}$ complex, and collected and processed the negative-stain electron microscope data for that complex. F.G., assisted by A.D., purified the $T4SS_{3-10}$ complex and performed the stoichiometry, gold labelling and membrane wash experiments for that complex. A.R.-C. purified, collected electron microscope data and processed the TrwH/TrwF/TrwE complex. N.B., assisted by A.R., collected $T4SS_{3-10}$ complex cryo-negative-stain data. H.H.L. and A.R.-C. purified, collected electron microscope data and processed TrwK and MBP–TrwK. A.R.-C. and F.L. purified the TrwM/TrwK complex and determined its stoichiometry. H.H.L. drafted the paper, and H.H.L., F.G., R.F., E.V.O. and GW finalized it.

Author Information The electron microscope composite map of the $T4SS_{3-10}$ complex has been deposited in the Electron Microscopy Data Bank under accession number EMD-2567. Reprints and permissions information is available at www.nature.com/reprints. The authors declare no competing financial interests. Readers are welcome to comment on the online version of the paper. Correspondence and requests for materials should be addressed to G.W. (g.waksman@mail.cryst.bbk.ac.uk), E.V.O. (e.orlova@mail.cryst.bbk.ac.uk) or R.F. (remi.fronzes@pasteur.fr).

METHODS

Molecular biology. Cloning of the R388 plasmid from virB1/trwN to virB10/trwE ($T4SS_{1-10}$). The *trw* operon region of *E. coli* R388 plasmid from *virB1/trwN* to *virB10/trwE* (*$T4SS_{1-10}$*) was amplified by PCR and cloned into both IBA-GO pASK3c (pASK3c:*$T4SS_{1-10}$*) and pBAD-M11 (pBAD:*$T4SS_{1-10}$*) expression vectors using a commercial kit based on homologous recombination (Clontech In-Fusion). In both constructs, a sequence encoding the StrepII tag was incorporated at the 3′ terminus of *virB10/trwE*. The clone pASK3c:*$T4SS_{1-10}$* was used for the overexpression and purification of the $T4SS_{3-10}$ complex, whereas pBAD:*$T4SS_{1-10}$* was used for the purification of the $T4SS_{3-10/B4\text{-}His6}$ (used for gold labelling experiments) and $T4SS_{3-10/His6\text{-}B6}$ (used for iodine-125 labelling and gold labelling experiments) complexes once the respective tags had been added (see below).

His-, Flag- and MBP derivations of the $T4SS_{1-10}$ clones. For iodine-125 labelling and gold labelling, a His_6 tag was incorporated at the N terminus of VirB6/TrwI (pBAD:*$T4SS_{1-10/His6-B6}$*) or the C terminus of VirB4/TrwK (pBAD:*$T4SS_{1-10/B4-His6}$*) using a Stratagene QuikChange or Clontech In-Fusion kit. A MBP insert from *E. coli* was similarly added to the N terminus of VirB4/TrwK within pASK3c:*$T4SS_{1-10}$* to generate pASK3c:*$T4SS_{1-10/MBP-B4}$*. For western blots that tested the presence of specific Trw proteins within the $T4SS_{3-10}$ complex, Flag and His_6 tags were incorporated into pASK3c:*$T4SS_{1-10}$* as specified in the main text and Extended Data Fig. 1b.

Cloning of the virB3/TrwM–VirB4/trwK complex. *virB3/trwM* and *virB4/trwK* insert amplified from pASK3c:*$T4SS_{1-10}$*, and generated with BsaI restriction enzyme sites at each end, was digested with BsaI and ligated into similarly cut pASK3c vector. A sequence encoding the strepII tag was therefore located at the 3′ terminus of *virB4/trwK* (pASK3c:*$T4SS_{3-4}$*).

Cloning of virB7/trwH–virB10/trwE. The *trw* operon region composed of *virB7/trwH*, *virB8/trwG*, *virB9/trwF* and *virB10/trwE* from R388 plasmid was cloned into pASK3c as for the cloning of the pKM101 *traN* to *traF* gene cluster[1]. A sequence encoding the StrepII tag was therefore located at the 3′ end of *virB10/trwE*. This plasmid (pASK3c:*$T4SS_{7-10}$*) was used for the expression of the R388 core complex.

Protein overexpression and purification. Purification of the $T4SS_{3-10}$ complex. pASK3c:*$T4SS_{1-10}$* was transformed into *E. coli* BL21 Star (DE3) strain (Invitrogen), and grown at 35 °C in synthetic M9 minimal media supplemented with glucose, vitamins and amino acids (except methionine) (Molecular Dimensions). L-methionine was added separately (0.1 g l^{-1}). At absorbance $A_{600\,nm} = 0.6$, cells were induced using anhydrotetracycline (AHT, 0.2 mg l^{-1}) and the temperature dropped to 19 °C. Cells were collected approximately 15 h later and were used immediately. Pellets were re-suspended in cooled 50 mM Tris-HCl pH 8.0, treated with DNase I, lysozyme and EDTA-free protease inhibitor tablets (Roche), and sonicated on ice. After cells were opened, 1 mM DTT and 1 mM EDTA was added, and the lysate clarified by centrifugation at 38,500*g* for 20 min. The membrane fraction was then collected by centrifugation at 98,000*g* for 45 min. Membranes were mechanically homogenized and solubilized in 50 mM Tris-HCl pH 8.0, 200 mM NaCl, 0.5% w/v DDM (Anatrace), 0.75% w/v DM-NPG (Anatrace), 0.1% w/v digitonin (Sigma-Aldrich), 1 mM DTT and 1 mM EDTA at room temperature for 40 min. The suspension was clarified by centrifugation at 98,000*g* for 20 min. The supernatant was loaded onto a 1 ml StrepTrap HP (GE Healthcare) column and then washed with 50 mM Tris-HCl pH 8.0, 200 mM NaCl, 0.06% w/v DM-NPG, 0.1% w/v digitonin, 1 mM DTT and 1 mM EDTA at 4 °C. The purified $T4SS_{3-10}$ complex was eluted in the equivalent wash buffer supplemented with 2.5 mM desthiobiotin (IBA). The sample was used immediately for electron microscopy.

Purification of the R388 core complex. The core complex purification using pASK3c:*$T4SS_{7-10}$* was as described in ref. 7 with minor modification. BL21 (DE3) (Invitrogen) cells were grown at 37 °C until induced with AHT at $A_{600\,nm} = 0.65$. After approximately 15 h at 16 °C, cells were collected by centrifugation and opened using an emulsiflex-C5 (Avestin). The cooled lysate was clarified by initial centrifugation at 38,500*g* for 15 min, then the membrane fraction was collected by centrifugation at 98,000*g* for 45 min. This membrane fraction was solubilized in 50 mM Tris-HCl pH 8.0, 50 mM NaCl, 1 mM EDTA, 10 mM *N*,*N*-dimethyl-1-dodecanamine-*N*-oxide (LDAO, Anatrace) and 1% w/v DDM at room temperature for 1 h. Insoluble material was removed by centrifugation at 98,500*g* for 15 min. The supernatant was loaded onto a pre-equilibrated StrepTrap HP and washed with 50 mM Tris-HCl pH 8.0, 200 mM NaCl, 10 mM LDAO at 4 °C. Elution was with the same buffer supplemented with 2.5 mM desthiobiotin. Peak fractions were pooled, concentrated and loaded onto a Superose 6 10/300 column (GE Healthcare) equilibrated in 50 mM Tris-HCl pH 8.0, 600 mM NaCl, 10 mM LDAO. The fractions containing the core complex were pooled and concentrated.

Purification of the $T4SS_{3-10/His6\text{-}B6}$ and $T4SS_{3-10/B4\text{-}His6}$ complexes. TOP10 strain (Invitrogen) was used to express pBAD:*$T4SS_{1-10/His6-B6}$* or pBAD:*$T4SS_{1-10/B4-His6}$* in Luria broth media. Transformation and pre-culture was performed in the presence of 0.4% w/w glucose to minimize leaking expression. To eliminate traces of glucose from the pre-culture, cells were washed by centrifugation and re-suspended in fresh LB before starting the large-scale culture. At $A_{600\,nm} = 0.6$ cells were incubated at 16 °C, and at $A_{600\,nm} = 0.9$ cells were induced with addition of 0.08% w/v arabinose and collected after approximately 15 h. Purification of each complex then proceeded as for the $T4SS_{3-10}$ complex. However, after elution from the streptactin column, the eluate was passed through a 1 ml HisTrap affinity column (GE Healthcare), washed with 50 mM Tris-HCl pH 8.0, 200 mM NaCl, 0.06% w/v DM-NPG, 0.1% w/v digitonin, 1 mM DTT and 1 mM EDTA supplemented with 50 mM imidazole, and eluted in the presence of 350 mM imidazole.

Purification of the VirB3/TrwM–VirB4/TrwK complex. TOP10 cells transformed with pASK3c:*$T4SS_{3-4}$* were grown in LB broth at 37 °C until $A_{600\,nm} = 0.65$. Cells were then induced using AHT (0.2 mg l^{-1}) and the temperature dropped to 18 °C. Cells were collected approximately 15 h later and used immediately. Pellets were re-suspended in cooled 50 mM Tris-HCl pH 8.0, treated with DNase I, lysozyme and EDTA-free protease inhibitor tablets, and sonicated on ice. After cells were opened, the lysate was clarified by centrifugation at 38,500*g* for 20 min. The membrane fraction was then collected by centrifugation at 98,000*g* for 45 min. Membranes were mechanically homogenized and solubilized in 50 mM Tris-HCl pH 7.2, 150 mM NaCl, 1 mM EDTA, 1 mM DTT, 10 mM LDAO, 1% w/v DDM and EDTA-free protease inhibitor tablets at 4 °C for 45 min. The suspension was clarified by centrifugation at 38,500*g* for 15 min. The supernatant was loaded onto a StrepTrap HP equilibrated in 50 mM Tris-HCl pH 7.2, 150 mM NaCl, 1 mM LDAO, 1 mM EDTA, 1 mM DTT. The column was first washed and then eluted with the same buffer supplemented with 2.5 mM desthiobiotin. Fractions containing VirB3/TrwM and VirB4/TrwK were pooled together and loaded onto a HiTrapQ HP (GE Healthcare) to remove bound DNA. After washing with 50 mM Tris-HCl pH 7.2, 150 mM NaCl, 1 mM LDAO, 1 mM EDTA and 1 mM DTT, samples were eluted with a linear gradient of the same buffer supplemented with 1 M NaCl. Fractions containing VirB3/TrwM and VirB4/TrwK were loaded onto a Superose 6 10/300 equilibrated in 50 mM Tris-HCl pH 7.2, 150 mM NaCl, 1 mM LDAO, 1 mM EDTA, 1 mM DTT. The gel filtration profile consisted of two characteristic peaks: one corresponding to the oligomeric complex of VirB3/TrwM–VirB4/TrwK, the other containing only VirB4/TrwK. To identify the molar ratio of VirB3/TrwM–VirB4/TrwK in the oligomeric peak, corresponding fractions were analysed by SDS–PAGE and the gels stained with SYPRO Ruby (Bio-Rad). Gel bands were scanned using a Fujifilm FLA-300 scanner and band intensity analysed with the ImageJ software[25].

Purification of VirB4/TrwK. BL21(DE3) cells transformed with pASK3c:*$T4SS_{3-4}$* were used for overexpression and purification of VirB4/TrwK from the membrane fraction. Note that BL21(DE3) cells did not express VirB3/TrwM although they did express VirB4/TrwK. Purification of VirB4/TrwK was performed as described for the VirB3/TrwM–VirB4/TrwK complex including some minor modifications. After membrane solubilization and clarification of the solubilized fraction by centrifugation, the supernatant was loaded onto a StrepTrap HP equilibrated in 50 mM Tris-HCl pH 7.2, 150 mM NaCl, 1 mM LDAO, 1 mM EDTA, 1 mM DTT. The eluted sample was then loaded onto a Superose 6 10/300 equilibrated in the same buffer. The only peak on the gel filtration profile corresponded to VirB4/TrwK, and the calculation of its molecular mass used a Superdex 200 (GE Healthcare) calibrated with high molecular mass standards (Bio-Rad). The purified monomeric VirB4/TrwK was used for subsequent electron microscopy.

Purification of N-terminal MBP–VirB4/TrwK fusion protein. BL21 Star (DE3) cells transformed with pASK3c:*$T4SS_{1-10/MBP-B4}$* were grown at 35 °C in synthetic M9 minimal media supplemented with glucose, vitamins and amino acids. L-Methionine was added separately (100 mg l^{-1}). At $A_{600\,nm} = 0.4$, cells were induced using AHT (0.2 mg l^{-1}) and the temperature dropped to 19 °C. Cells were collected approximately 15 h later. Pellets were re-suspended in cooled buffer containing 50 mM Tris-HCl pH 8.0, 200 mM NaCl, treated with DNase I, lysozyme and EDTA-free protease inhibitor tablets (Roche), and sonicated on ice. After cells were opened, the lysate was clarified by initial centrifugation at 38,500*g* for 20 min, then subjected to centrifugation at 98,000*g* for 45 min. The resulting supernatant was loaded onto a pre-equilibrated column consisting of amylose resin (New England Biolabs). The column was washed with 50 mM Tris-HCl pH 6.5, 150 mM NaCl, 50 mM potassium acetate, 5% glycerol at 4 °C. Peak fractions were concentrated using a Vivaspin concentrator with 50 kDa molecular mass cutoff and then loaded onto a Superose 6 10/300 gel filtration column equilibrated in 20 mM PIPES sodium salt-HCl pH 6.5, 100 mM NaCl, 75 mM potassium acetate, 10 mM magnesium acetate, 5% glycerol, 0.1 mM EDTA. These buffers were derived from the VirB4/TrwK purification strategy described in (ref. 13). After gel filtration there were still trace contaminants so peak fractions were diluted in 50 mM Tris-HCl pH 8.0, 25 mM NaCl, 1 mM EDTA, 1 mM DTT and loaded onto a HiTrap Q HP (GE Healthcare). Elution of a single purified peak was by gradient against the same buffer supplemented with 1 M NaCl.

Electron microscopy and image processing. Determination of $T4SS_{3-10}$ complex structure. Owing to the high contrast of negative-stain electron microscopy images over those obtained from unstained vitrified samples, negative-stain electron

microscopy was selected as the method of choice. High-contrast images allowed particle quality to be judged before manual picking and aided the alignment of the picked particles during processing steps. The determination of the *de novo* $T4SS_{3-10}$ complex structure by negative-stain electron microscopy and a thorough understanding of general features and local symmetry were deemed requisite before future succession to cryo-electron microscopy. Concerns over the possibility of structural distortion due to the effect of particle drying and flattening during the negative-stain procedure were eliminated by validating negatively stained $T4SS_{3-10}$ complex images against the equivalent obtained using a limited cryo-negative-stain tilt series.

Negative-stain electron microscopy structure of the $T4SS_{3-10}$ complex. Three microlitres of suitably diluted (~0.01 mg ml^{-1}) $T4SS_{3-10}$ complex sample was applied to glow-discharged carbon-coated copper grids (Agar Scientific). After incubation for 30 s, the sample was blotted, washed with three drops of water and then stained with 2% uranyl acetate. Images were recorded on an Gatan UltraScan 4000 CCD camera (Gatan) with low electron dose (~25 e Å^{-2}) on a Tecnai F20 FEG microscope operating at a voltage of 200 kV, a magnification of about 45,500 (3.3 Å per pixel) and a defocus range of 0.8–2.0 μm. A total of 21,680 particles, judged to be evenly stained and non-aggregated, were manually selected from 693 frames and extracted within boxes of 192 pixels × 192 pixels using EMAN/BOXER[19]. The CTF was estimated using CTFFIND3 (ref. 20) and correction was done by phase flipping using BSOFT[21]. Images of particles were normalized, band-pass filtered, centred, subjected to reference-free MSA[22] and classified with approximately 20 images per class. The particle images were further aligned and classified by several rounds of multi-reference alignment (MRA)[22], where the best classes representing characteristic views were used as new references, followed by MSA. A subset of representative class averages (with low variance within classes) were assigned Euler angles by angular reconstitution[22] using the reconstruction of the pKM101 core complex bound to VirB4/TraB (Electron Microscopy Data Bank accession numbers EMD-2136 and EMD-2137)[10] as a starting model (in this model, VirB4/TraB confers asymmetry to the core complex base). An initial asymmetric (no symmetry imposed) three-dimensional reconstruction of the entire $T4SS_{3-10}$ complex was then generated. This initial map was improved using anchor set refinement interspersed with rounds of MRA and classification to produce a three-dimensional reconstruction of the entire $T4SS_{3-10}$ complex. For image processing, MSA, determination of angular orientations by angular reconstitution and three-dimensional reconstruction and structure refinement were performed using IMAGIC[23], whereas image alignments used SPIDER[24]. Flexibility between the core complex and the IMC prevented further improvement of the reconstruction, restricting particle alignment and ultimately the final resolution of the three-dimensional reconstruction (Extended Data Fig. 3a–c). Thus, we performed a separate analysis for the core complex and the IMC. Here, the three-dimensional reconstruction of the entire complex was shifted down or up so that either the core complex/stalk sub-region or the IMC sub-region became centred, respectively. These sub-regions were then individually spherically masked to create two sub-structures that were used as starting models to generate higher resolution reconstructions of the two sub-regions as described below.

Core complex/stalk sub-region reconstruction refinement. The aligned image stack was shifted using the same downward shift that was applied to centre the low-resolution core complex sub-structure (see above), and a circular mask applied. The core complex sub-region was then refined by the iterative procedure of MRA and classification, reducing the number of images per class to between three and four, followed by refinement of angular orientation using the reconstruction from the previous iteration. C_{14} symmetry was periodically applied during reconstruction although this was restricted to the O-layer and cap regions of the core complex, so that asymmetric details in the I-layer and stalk should be preserved. To assess map resolution, the classes were divided into two groups (even and odd). No symmetry was applied during the final steps of the reconstruction refinement, which achieved a resolution of 18 Å as determined by Fourier shell correlation at a threshold of 0.5 using 2,500 class averages (Extended Data Fig. 4a).

IMC sub-region reconstruction refinement. The original aligned stack was shifted but this time using the upward shift applied to centre the low-resolution IMC sub-region reconstruction (described above), and a circular mask applied. The IMC sub-region was then refined in the same way as described for the core complex sub-region. The first asymmetrical reconstruction clearly demonstrated features corresponding to C_2 symmetry with a self cross-correlation in the non-symmetrized volume of about 80%. C_2 symmetry was applied periodically during processing of data. Towards the end of refinement, SPIDER was used for projection matching of class averages instead of angular reconstitution, along with three-dimensional reconstruction. Projection matching, in particular the SPIDER back projection algorithm, yielded marginally improved resolution. As above, the classes were divided into two groups (even and odd) to assess map resolution. No symmetry was applied to the final reconstruction, which achieved a resolution of 23 Å as determined by Fourier shell correlation at a threshold of 0.5 correlation (Extended Data Fig. 4a) using 803 class averages.

Generation of the composite $T4SS_{3-10}$ map. The two discrete maps of the core complex/stalk and IMC were normalized to have equivalent standard deviation (σ) of densities, then overlaid after applying in reverse the shifts initially applied to the core or IMC sub-regions (see above). Local alignment of the two structures was then optimized using the 'Fit in Map' function in Chimera[26]. Redundant regions of overlap between the two reconstructions were then masked as delineated in Fig. 3b to yield the final composite map. The density threshold for surface rendering of the composite $T4SS_{3-10}$ map was chosen based on the fit of the outer-membrane complex crystal structure[12] within the core complex, which corresponded to a threshold of 0.64σ. Based on this threshold and a volume/mass conversion of 0.81 Da Å^{-3}, the $T4SS_{3-10}$ map has a calculated mass of approximately 3.0 MDa.

Assessment of the flexibility between the core complex and the IMC in the $T4SS_{3-10}$ complex. The angular variation between the core complex and the IMC was assessed using class averages that represent the 'front' view of the entire complex. $T4SS_{3-10}$ complex class averages with the core complex masked out were aligned to a typical IMC 'front' view. For each of the top 15 representative unmasked, aligned 'front' views (as assessed by the cross-correlation), the angle between the core complex and the IMC was measured by projection matching against back projections of a reference core complex structure. The distribution plot for these angles is shown in Extended Data Fig. 3c.

Cryo-negative staining of the $T4SS_{3-10}$ complex. Fresh $T4SS_{3-10}$ complex sample (3 μl at ~0.01 mg ml^{-1}) was applied for 2 min to glow-discharged holey carbon-coated copper grids (Quantifoil) covered with a thin film of carbon, and stained with ammonium molybdate (pH 7.5)[27] at saturated concentration before vitrification. Fifteen tilt series (each consisting of three tilt angles (−40°, 0°, 40°)) were recorded under low-dose conditions (~10 e Å^{-2}) with an FEI Tecnai F20 FEG microscope operating at a voltage of 200 kV, a magnification of 68,200 (2.2 Å per pixel) and a defocus range of 2.5–3.5 μm. One hundred and forty-one evenly stained and non-aggregated particles were selected and tracked over the three tilt angles. Boxed images were normalized, band-pass filtered and centred. Two representative particles with their long axis coinciding with the tilt axis are shown in Extended Data Fig. 6. All images from different tilt angles were also combined in one stack and processed as described above to generate a limited set of class averages (five images per class), some of them shown in Extended Data Fig. 6.

Crystal structure fitting. The docking of the outer-membrane complex crystal structure was performed by manual fitting with automated local refinement in Chimera. Segmentation of the $T4SS_{3-10}$ complex was performed as part of the Segger package in Chimera. For the docking of the VirB4 C-terminal ATPase domain from *T. pseudethanolicus*, two monomers were first superimposed onto two neighbouring subunits of the related TrwB hexameric crystal structure (1GL6) to create a dimer. Three such dimers per segmented IMC barrel were then manually fitted with automated local refinement in Chimera.

Electron microscopy and image processing of the R388 core complex. Three microlitres of the purified complex diluted to 0.04 mg ml^{-1} was applied to glow-discharged carbon-coated grids (Agar Scientific). Triton X-100 was added at a final concentration of 0.1% to increase the number of side views. The sample was negatively stained with 2% uranyl acetate and visualized in an FEI Tecnai F20 FEG microscope operating at a voltage of 200 kV under low-dose conditions (~25 e Å^{-2}). Images were recorded as described above at a magnification of 68,200 (2.2 Å per pixel) and a defocus range of 0.8–2.0 μm. Images were corrected for the CTF effect as described above and 1,981 particles selected manually using BOXER. Images were normalized, band-pass filtered and centred using EMAN. They were then subjected to a reference-free classification using EMAN. The images corresponding to end and side views were extracted into two separate subsets containing 638 and 368 single particle images, respectively. End views were further aligned and classified using MLalign2D (XMIPP)[28]. The final classes were checked for symmetry by calculating their rotational auto-correlation function as described previously[7]. A plot of the rotational auto-correlation function showed 14 peaks reflecting the C_{14} symmetry of the core complex (Extended Data Fig. 2d).

Electron microscopy and image processing of the $T4SS_{3-10/His6-B6}$ complex. Fresh purified complex (4 μl at ~0.01 mg ml^{-1}) was applied to glow-discharged carbon-coated grids (CF-400, Electron Microscopy Sciences). The sample was negatively stained with 2% uranyl acetate and visualized in an FEI Tecnai T12 BioTWIN LaB6 microscope operating at a voltage of 120 kV. Images were recorded on an FEI Eagle 4Kx4K CCD camera under low-dose conditions (~25 e Å^{-2}) at a magnification of about 44,000 (3.4 Å per pixel) and a defocus range of 1–2.5 μm. The CTF parameters were assessed from entire image frames using CTFFIND3. Phase flipping used SPIDER and was applied to entire frames. A total of 1,284 particles were selected manually from CTF-corrected micrographs using BOXER (EMAN2). Boxed images were normalized, band-pass filtered and centred. They were then subjected to a reference-free classification. Iterations of MRA using

representative views of the complex and MSA were performed in IMAGIC until the classification of the data set stabilized. The final classes were generated with approximately 20 images per class.

Electron microscopy and image processing of VirB4/TrwK and MBP–VirB4/TrwK fusion protein. Three microlitres of the purified VirB4/TrwK or MBP–VirB4/TrwK fusion protein diluted to 0.01 mg ml^{-1} were applied to glow-discharged carbon-coated grids (Agar Scientific). The sample was negatively stained with 2% uranyl acetate and observed in an FEI Tecnai F20 FEG microscope operating at a voltage of 200 kV. Images were recorded on a Gatan CCD camera (as for the $T4SS_{3-10}$ complex) under low-dose conditions (~10 e Å^{-2}) at a magnification of 104,167 (1.44 Å per pixel) and a defocus range of 1–2.5 μm. Images were CTF-corrected as described above, and 3,100 (VirB4/TrwK) or 4,569 (MBP–VirB4/TrwK) particles were selected manually using BOXER. Images were normalized, band-pass filtered and centred, subjected to a reference-free classification using EMAN, then classified using MLalign2D (XMIPP) and/or MRA with MSA (IMAGIC).

Gold labelling, stoichiometry and membrane washing experiments. VirB4/TrwK and VirB6/TrwI gold labelling. $T4SS_{3-10/B4\text{-}His6}$ or $T4SS_{3-10/His6\text{-}B6}$ complexes were applied onto a glow-discharged carbon coated grid (CF-400, Electron Microscopy Sciences). After 1 min, excess liquid was blotted, and the grid was washed on a drop of cold purification buffer (50 mM Tris pH 8, 200 mM NaCl, 1 mM TCEP, 0.1% w/v digitonin, 0.06% w/v DM-NPG) containing 50 mM imidazole, quickly blotted and deposited on a second drop of the same buffer in the presence of 5 nM nanogold beads (Nanoprobes). After 2 min, the grid was rinsed sequentially for 20 s with one drop of purification buffer, one drop of the same buffer without detergent and three drops of 2% uranyl acetate. Incubation was for 1 min. Images were collected on a Tecnai T12 BioTWIN LaB6 microscope operating at a voltage of 120 kV. Particles were selected manually using EMAN.

Stoichiometry determination by tyrosine labelling. Stoichiometry measurement was performed as in ref. 11 with modifications. $T4SS_{3-10/His6\text{-}B6}$ complex at a concentration ranging from 0.1 to 0.5 mg ml^{-1} was denatured by heating at 95 °C for 10 min in the presence of 1% SDS (final concentration). Stock solutions of 2 mg ml^{-1} chloramine-T and 3 mg ml^{-1} sodium metabisulphite were prepared in 20 mM triethylamine-HCl pH 7.5. To 52 μl of denatured protein, 1 μl of Na iodine-125 (at 100 μCi μl^{-1}) and 10 μl of 2 mg ml^{-1} chloramine-T were added and incubated for 2 min at room temperature under a hood. Reaction was quenched with 20 μl of sodium metabisulphite. Reaction mixture was dialysed at room temperature overnight against 50 mM Tris pH 8, 200 mM NaCl, 1% SDS to remove excess iodine-125. The percentage of iodine-125 incorporation was measured in a gamma counter as about 10%. SDS–PAGE was performed in Tricine 10% gels. About 3×10^6 counts per minute were loaded on each lane. The gel was fixed in 30% ethanol, 10% acetic acid solution overnight, then hydrated in 30% glycerol for 1 h and dried (Model 583 Biorad gel dryer) for 1 h at 60 °C on Whatman filter paper. Dried gels were exposed in a PhosphorImager (Molecular Dynamics) cassette for 1–3 h. Signal was analysed in a Storm 860 Molecular Imager with a pixel size of 50. For each lane, the density of each band was measured using Totallab Quant software (automatic band detection without background subtraction). Based on western blot and mass spectrometry results, we assigned each band to a VirB/Trw protein (Fig. 4). The signal obtained for each protein was then normalized according to the number of tyrosine residues it contained. VirB10/TrwE (stoichiometry of 14 copies per core complex) was used as a reference. The stoichiometry of the other proteins was determined by comparing their normalized signals with the one obtained for VirB10/TrwE. Reported means and corresponding standard deviations are from two separate labelling experiments on four independent preparations of the complex.

Membrane washing. Membranes from TOP10 cells transformed with pBAD: $T4SS_{3-10/B4\text{-}His6}$ complex were isolated as described above. The membrane pellet was re-suspended in 6 M urea and an aliquot collected for SDS–PAGE (lane 1, Extended Data Fig. 7f). Then membranes were collected by centrifugation at 98,000*g* for 45 min. The same procedure (pellet re-suspension, aliquot collection and centrifugation) was repeated, sequentially using 6 M urea, 100 mM sodium carbonate pH 11 and finally 2 M KCl as re-suspension buffers (lanes 2–4, Extended Data Fig. 7f). The last pellet was re-suspended in buffer (50 mM Tris pH 8.0, 200 mM NaCl) and collected for SDS–PAGE (lane 5, Extended Data Fig. 7f). The aliquots from each step were then analysed by western blot on nitrocellulose membrane. Anti-His_6 tag antibodies were used to detect the presence of VirB4/TrwK subunit in the membrane or soluble fractions.

25. Schneider, C. A., Rasband, W. S. & Eliceiri, K. W. NIH Image to ImageJ: 25 years of image analysis. *Nature Methods* **9,** 671–675 (2012).
26. Pettersen, E. F. *et al.* UCSF Chimera–a visualization system for exploratory research and analysis. *J. Comput. Chem.* **25,** 1605–1612 (2004).
27. De Carlo, S., Boisset, N. & Hoenger, A. High-resolution single-particle 3D analysis on GroEL prepared by cryo-negative staining. *Micron* **39,** 934–943 (2008).
28. Scheres, S. H. W., Nunez-Ramirez, R., Sorzano, C. O. S., Carazo, J. M. & Marabini, R. Image processing for electron microscopy single-particle analysis using XMIPP. *Nature Protocols* **3,** 977–990 (2008).
29. Orlov, S. S. Theory of three-dimensional reconstruction. 1. Conditions of a complete set of projections. *Sov. Phys. Crystallogr.* **20,** 312–314 (1975).
30. Kudryashev, M. *et al.* In situ structural analysis of the Yersinia enterocolitica injectisome. *eLife* **2,** e00792 (2013).

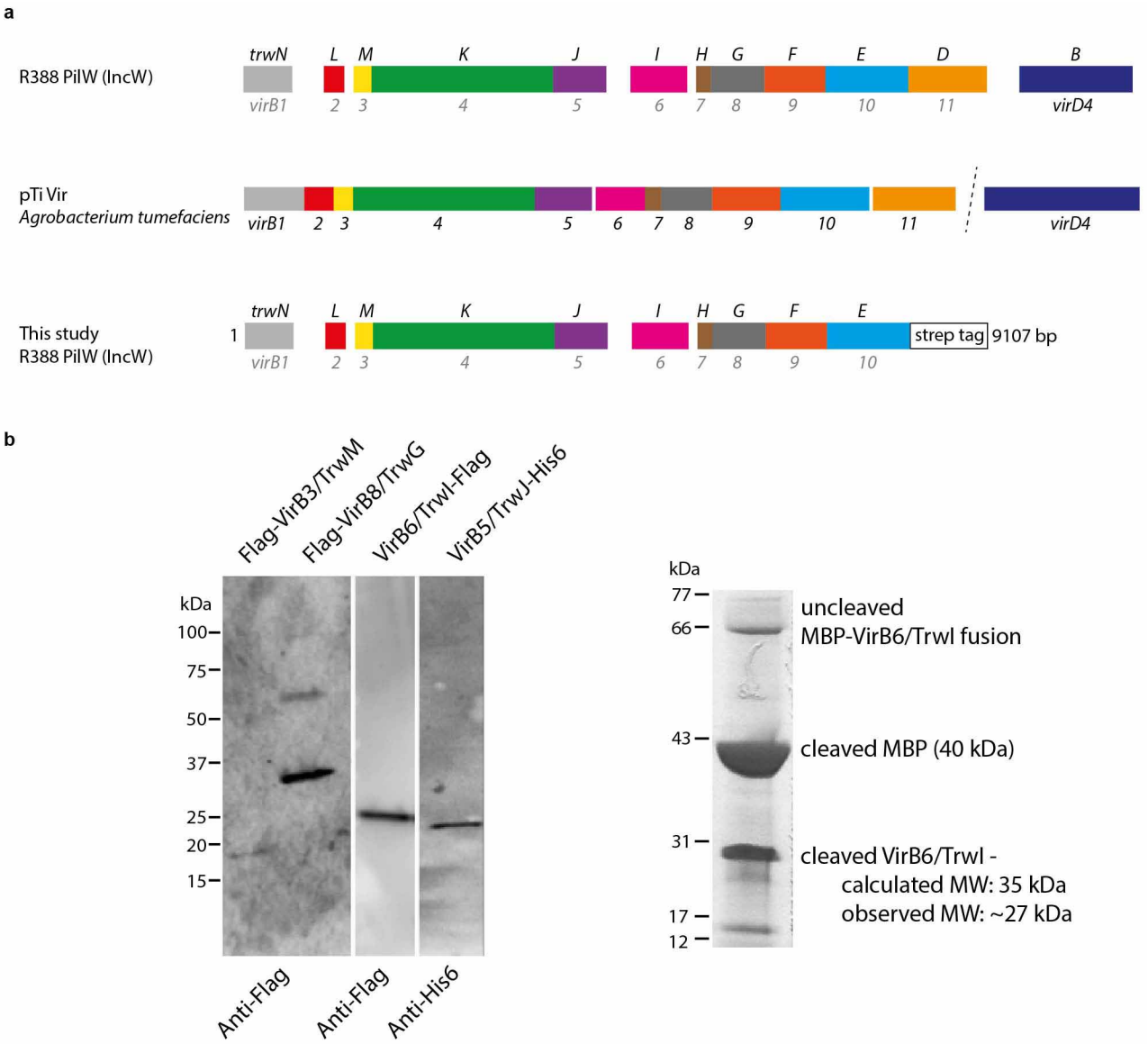

Extended Data Figure 1 | Conserved gene architecture between *E. coli* R388 plasmid and *A. tumefaciens* T4S systems. Confirmation of $T4SS_{3-10}$ complex constituents and the anomalous migration of VirB6/TrwI by SDS–PAGE. a, In this study, R388 *virB1/trwN* to *virB10/trwE* were overexpressed for purification of the $T4SS_{3-10}$ complex using a StrepII tag located at the VirB10/TrwE C terminus. The figure was adapted from ref. 2. **b**, Left, western blot of specific individually cloned His_6- or Flag-tagged gene variants in the *T4SS*$_{1-10}$ clone. Anti-His_6 or anti-Flag antibody was used as required. Note that western blot against Flag-tagged VirB2/TrwL in the purified $T4SS_{3-10}$ complex gel gave no signal. Also, extensive LC–MS of trypsin-digested $T4SS_{3-10}$ complex where VirB2 was untagged yielded no trace of VirB2/TrwL peptides. Thus, VirB2/TrwL could not be detected. VirB2/TrwL undergoes processing from a propilin to an assembly-competent pilin by a poorly understood mechanism that is reliant on signal peptidases and other poorly defined host encoded enzymes. Overexpression of such processing enzymes may therefore be required for overexpression of VirB2/TrwL and its incorporation into the $T4SS_{3-10}$ complex. However, another possibility for the failure to observe VirB2 is that VirB2 might not tolerate insertion of tags in its sequence. Note that a fully assembled $T4SS_{3-10}$ complex was observed by negative-stain electron microscopy for all His_6- or Flag-tagged variants investigated. Right, VirB6/TrwI purified in isolation as an N-terminal MBP fusion protein. Cleavage of MBP confirms that VirB6/TrwI migrates anomalously by SDS–PAGE with a mass of approximately 27 kDa rather than at 35.1 kDa as calculated from its sequence. This seems not to be a proteolysis product as western blot of C-terminal Flag-tagged VirB6/TrwI shows a similar migration pattern (left panel).

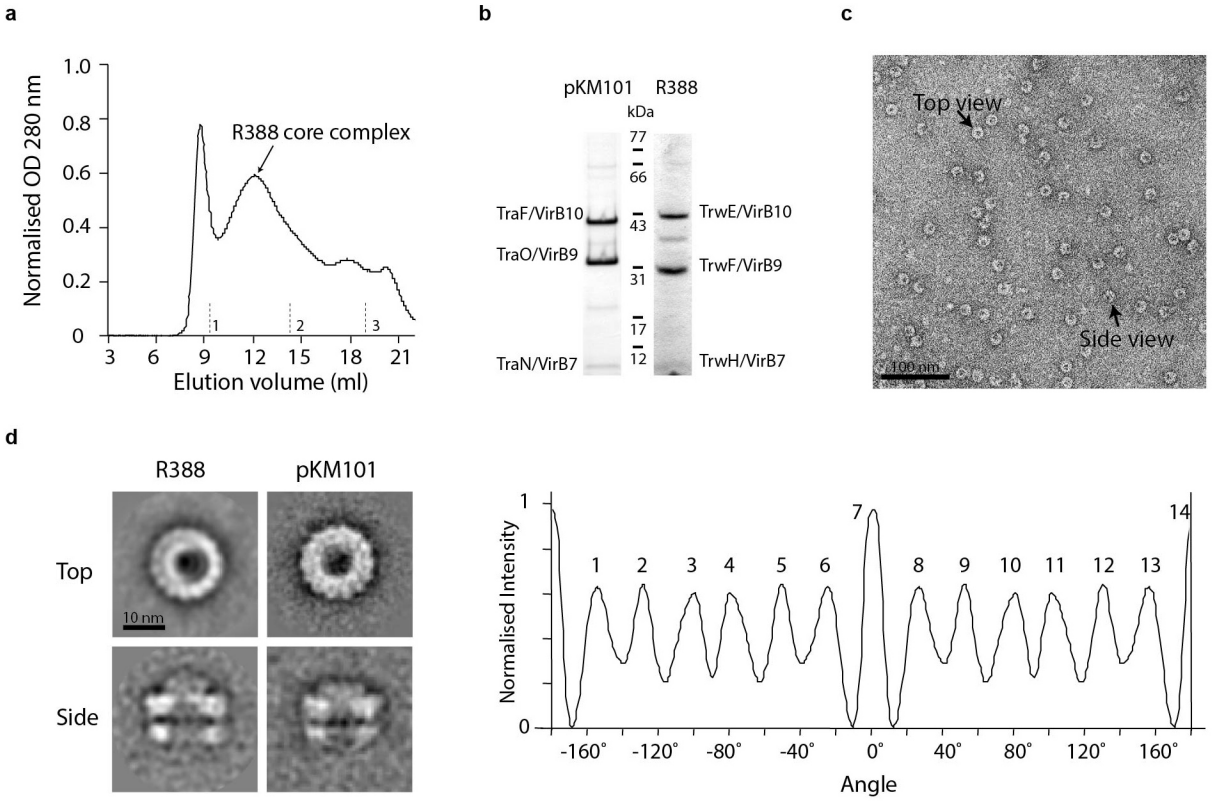

Extended Data Figure 2 | VirB10/TrwE, VirB9/TrwF and VirB7/TrwH form a pKM101-like core complex with C_{14} symmetry. **a**, VirB10/TrwE, VirB9/TrwF and VirB7/TrwH (the R388 core complex) co-elute as a single peak during gel filtration (1, column exclusion limit; 2, 665 kDa; 3, 75 kDa). **b**, SDS–PAGE comparison of pKM101 and R388 core complexes. VirB9/TrwF and VirB10/TrwE were confirmed by N-terminal sequencing. **c**, Typical negative-stain electron microscopy micrograph of R388 core complexes. **d**, Comparison of the R388 and pKM101 core complexes. Top and side view class averages for the two complexes (left panel). The R388 core complex shows clear C_{14} symmetry as shown by the rotational auto-correlation function plot (right panel).

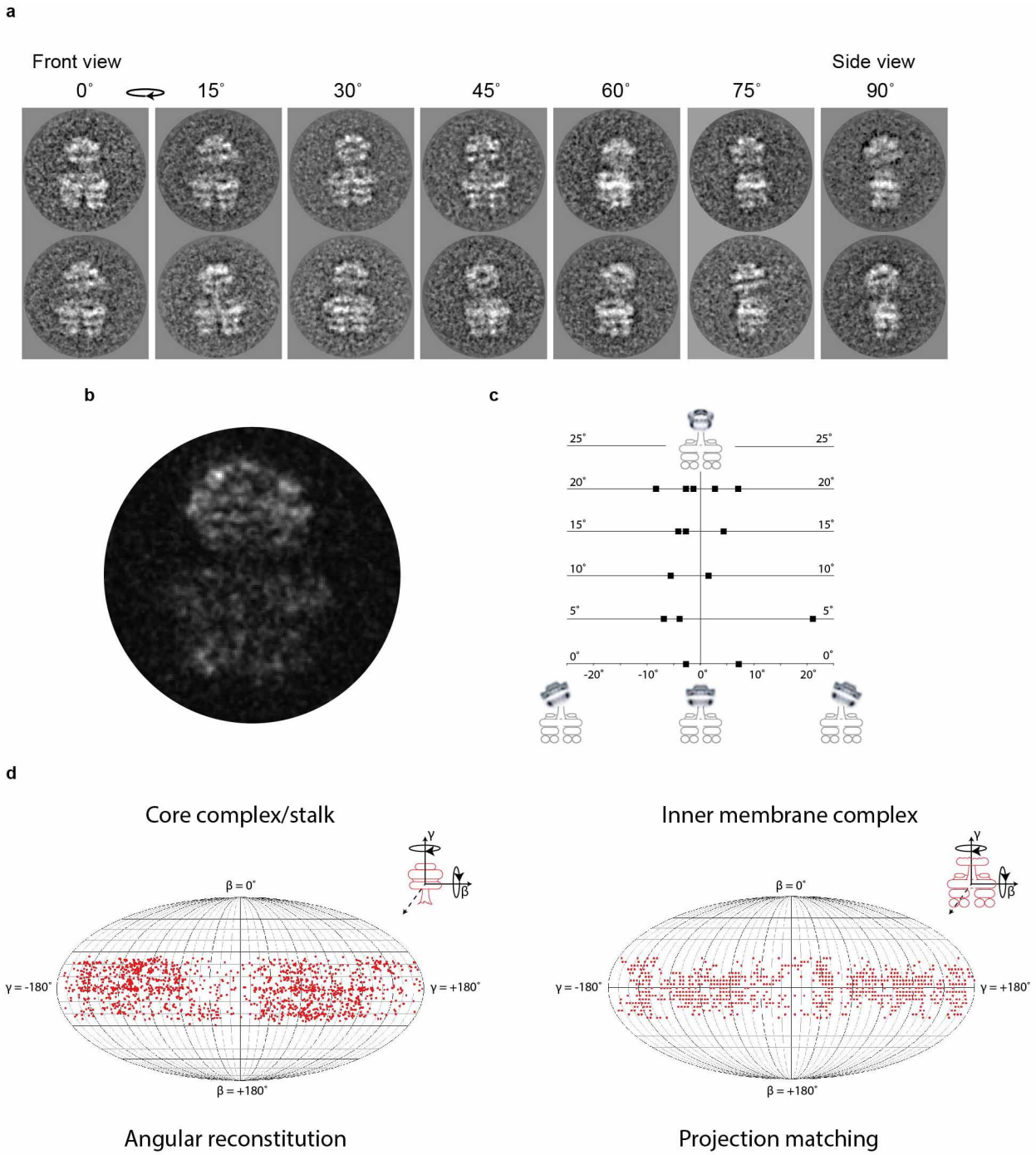

Extended Data Figure 3 | The T4SS$_{3-10}$ complex shows significant flexibility between the core complex and IMC. **a**, A gallery of pairs of typical T4SS$_{3-10}$ complex class averages chosen to show the IMC in 15° rotational increments around the particle long axis. Note the different tilts of the core complex in relation to the IMC. **b**, Variance analysis image to highlight observed flexibility between the core complex and IMC. The image shows the variance between 15 'front view' T4SS$_{3-10}$ complex class averages aligned using only their IMC region (see Methods for further detail). **c**, Angular distribution plot for the position of the core complex relative to the IMC. The plot consists of the same 15 'front view' T4SS$_{3-10}$ complex class averages as introduced in **b** (see Methods for further detail). **d**, Plots showing the assigned angular distribution of constituent classes around the Euler sphere for both the core complex/stalk and IMC reconstructions. Note that angular reconstitution was used for Euler angle assignment of the core complex/stalk, whereas projection matching was used for the IMC. The equatorial band distribution of angles reflects the fact that elongated molecules such as the T4SS$_{3-10}$ are mostly represented by side views. Such an even equatorial band distribution provides the basis for a reliable reconstruction as demonstrated in ref. 29.

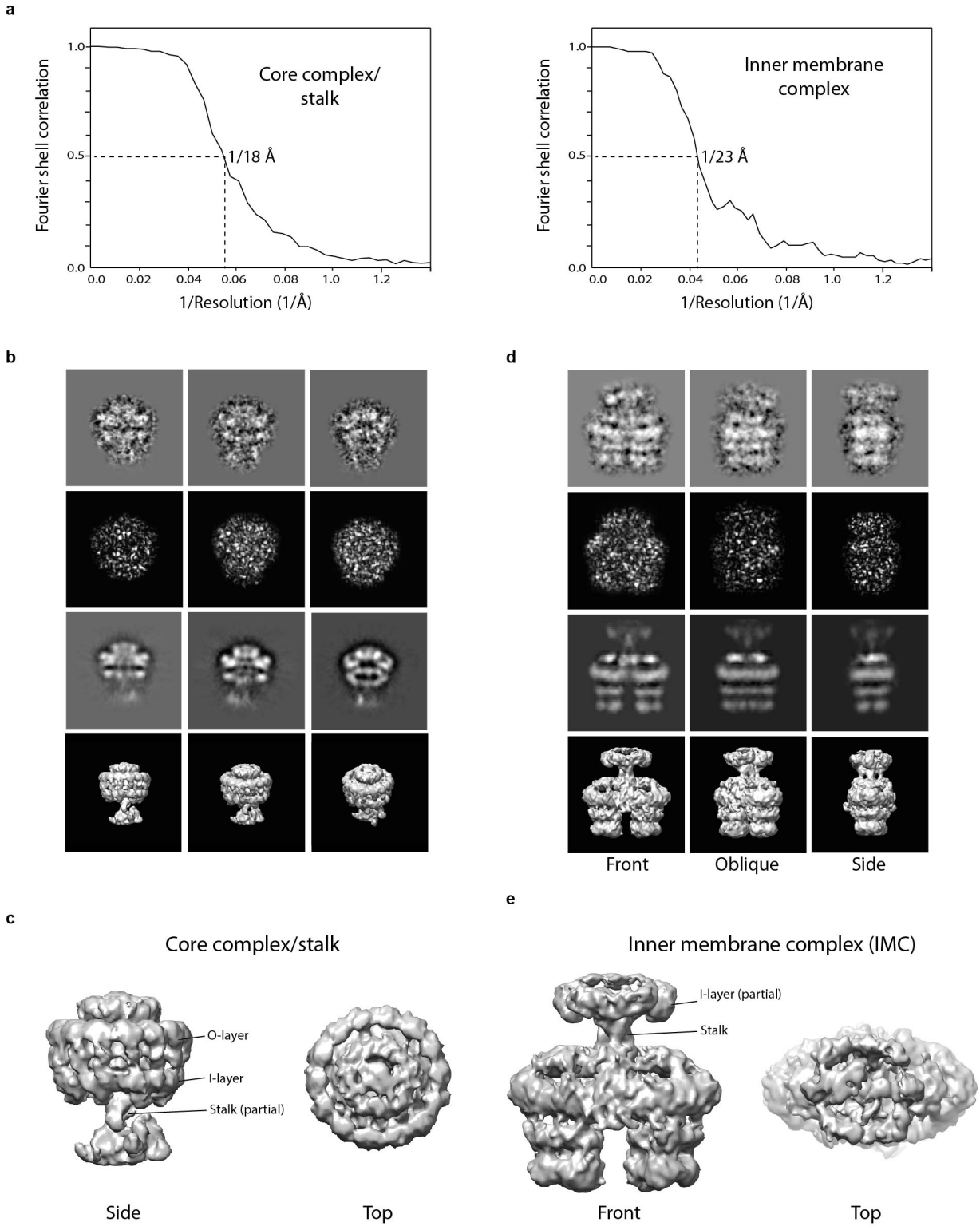

Extended Data Figure 4 | Fourier shell correlation and depiction of separate core complex and IMC reconstructions. **a**, Fourier shell correlation curves of the final models corresponding to the core complex (left) and IMC (right). Resolution according to the Fourier shell correlation = 0.5 criterion corresponds to approximately 18 and 23 Å, respectively. **b**, From top row to bottom row: representative class averages, respective variance images, corresponding re-projections and corresponding surface views of the final map for the core complex reconstruction. **c**, Side and top views of the core complex reconstruction. **d**, As described in **b**, but for the IMC reconstruction. **e**, Side and top views of the IMC reconstruction.

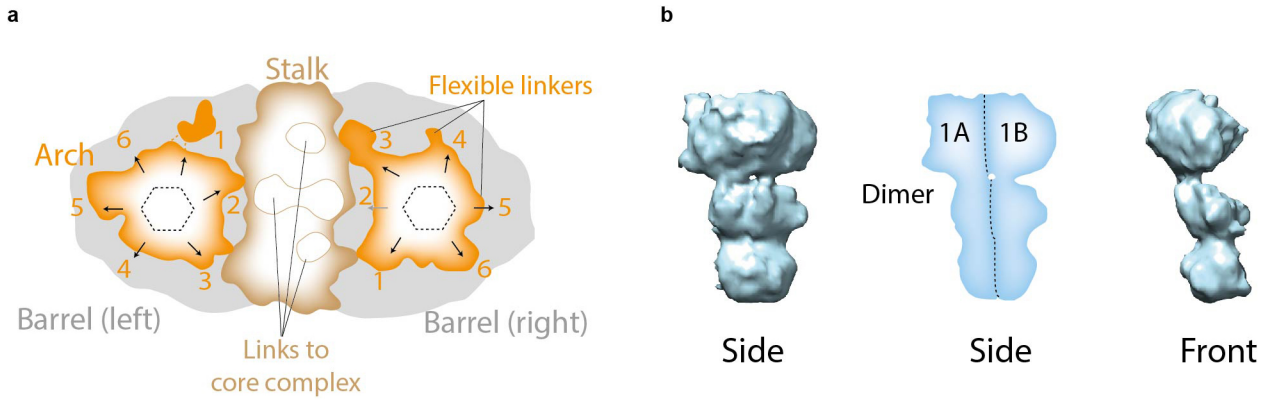

Extended Data Figure 5 | Schematic representation of components in selected regions of the T4SS$_{3-10}$ complex. **a**, Top view representation of the stalk and arches. In the asymmetric T4SS$_{3-10}$ complex reconstruction, four linkers are observed in the stalk. However, given the flexibility in this region, other unresolved linkers may exist. The arches are attached to the IMC barrels with up to six thin interconnecting flexible linkers (orange numerals, 1–6). The observed number of linkers varied during processing although a dominant triad was always observed in positions 1, 3 and 5. **b**, Surface representation and schematic (middle) of a single IMC barrel segment. Given the trimer of dimer arrangement of densities within the middle tier of each IMC barrel, each barrel segment (Fig. 3e) must consist of two subunits. The barrel densities comprise VirB4/TrwK as described in Fig. 4.

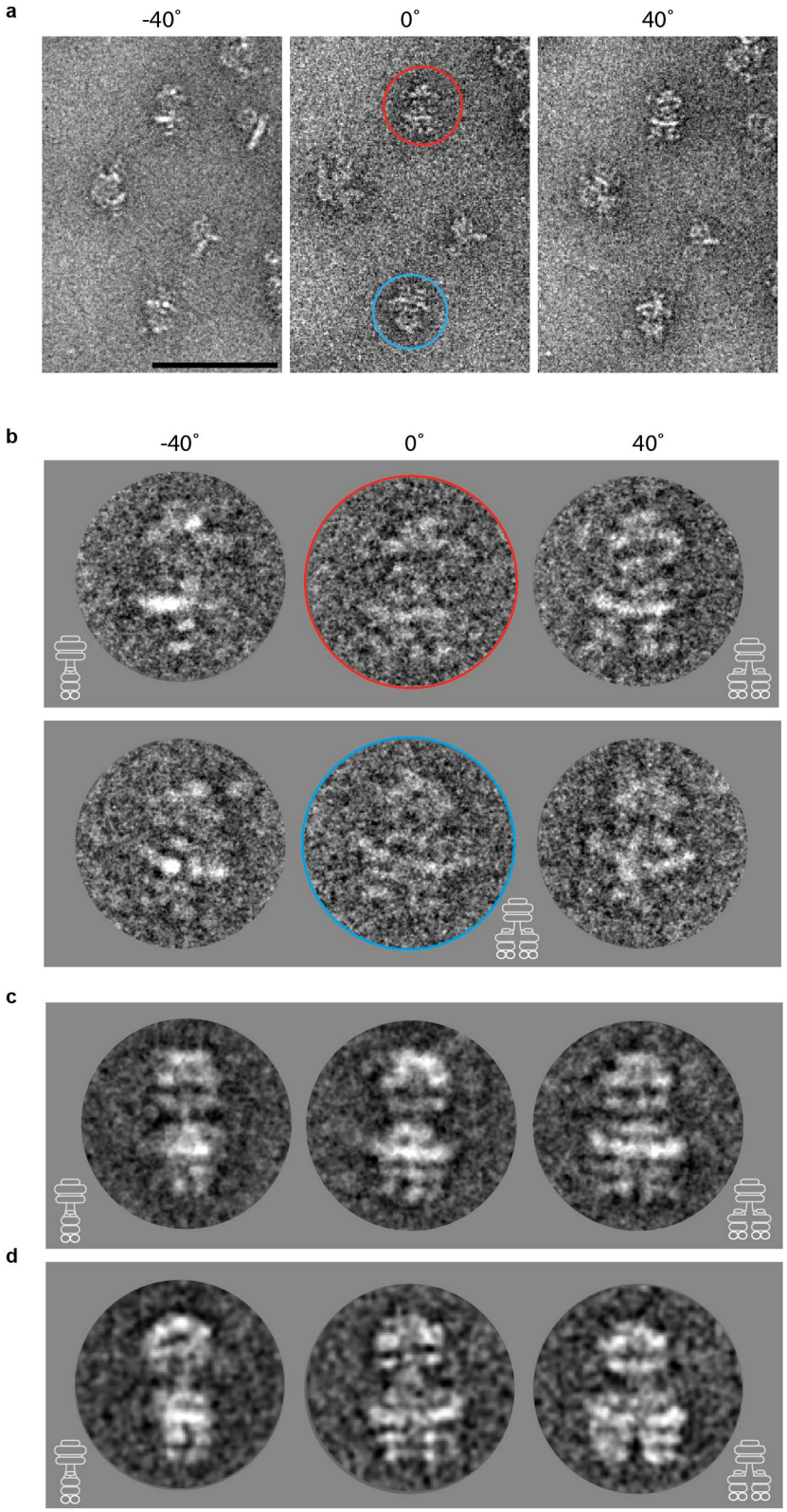

Extended Data Figure 6 | Verification of the T4SS$_{3-10}$ structure by cryo-negative staining. **a**, Three image tilt series of cryo-negatively stained T4SS$_{3-10}$ complexes. Scale bar, 100 nm. **b**, Tracking of specific individual particles (red or blue circle in **a**) at different tilt angles. Inset schematic diagrams aid interpretation of either side views (single barrel) or front views (two barrels). Note that the blue encircled particle has been rotated by about 180° in the image plane to show the particle with the core complex at the top. **c**, Representative characteristic class averages of cryo-negatively stained T4SS$_{3-10}$ complexes (from left to right: side, oblique and front views). **d**, Equivalent of **c**, but using negative stain.

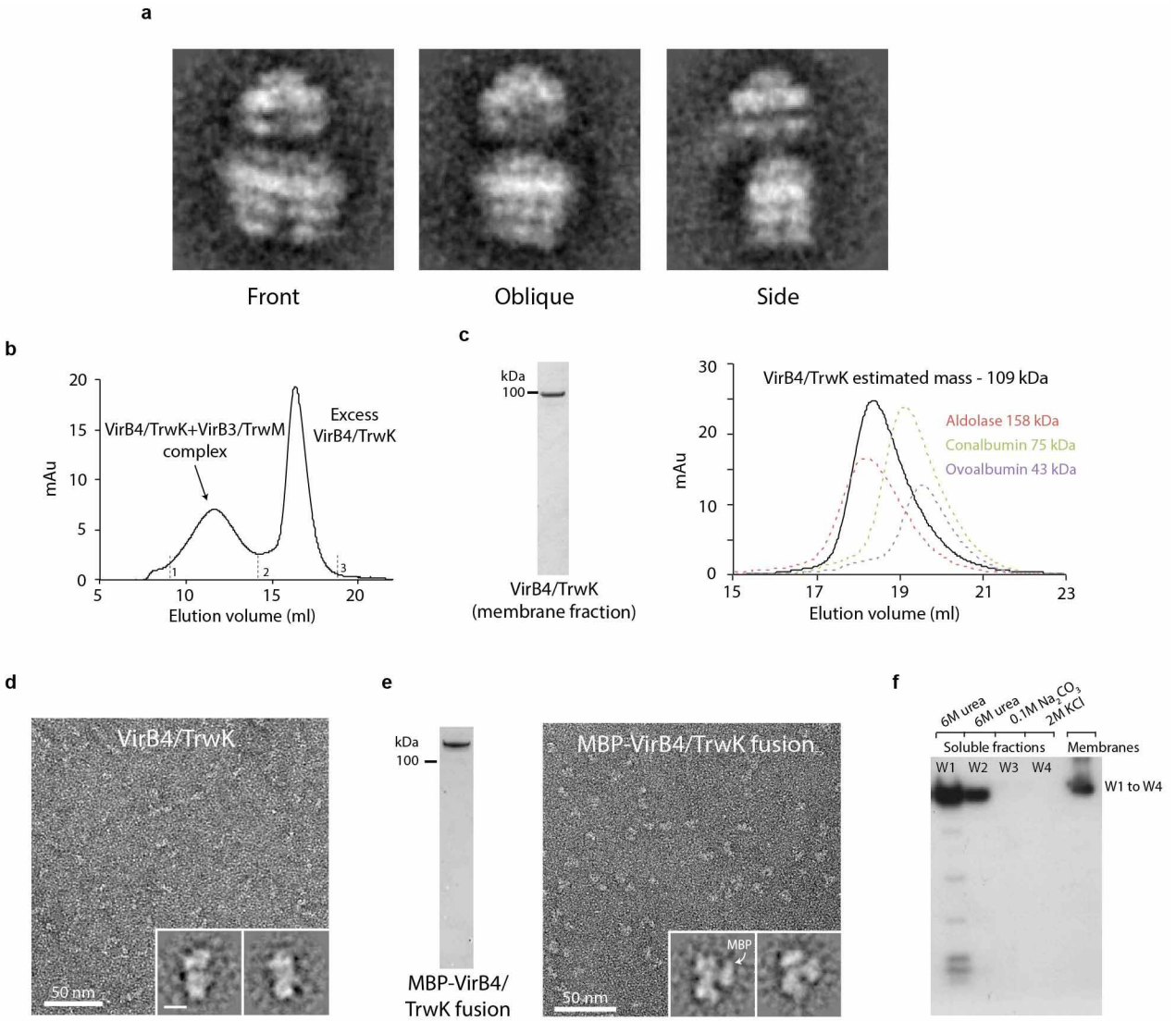

Extended Data Figure 7 | Class averages derived from a test data set of the $T4SS_{3-10/His6-B6}$ complex; biochemical and electron microscopy studies of VirB4/TrwK, and maltose binding protein (MBP) fused with VirB4/TrwK. **a**, Comparison of class averages of the $T4SS_{3-10/His6-B6}$ complex against those of the $T4SS_{3-10}$ complex show them to be similar. Views presented here are similar to those shown in Extended Data Fig. 3a at 0, 45 and 90°. **b**, Gel filtration profile showing the co-elution of a VirB4/TrwK and VirB3/TrwM complex (1, column exclusion limit; 2, 665 kDa; 3, 75 kDa). The SDS–PAGE of this complex is shown in Fig. 4B. **c**, Left, SDS–PAGE of VirB4/TrwK purified from the membrane fraction. Right, in the presence of LDAO detergent, VirB4/TrwK exists as a monomer as shown by size exclusion chromatography. **d**, Negative-stain electron microscopy image of VirB4/TrwK as purified in **c**. Class averages (inset) show monomeric VirB4/TrwK to form an elongated protein with general dimensions of approximately 105 Å × 40 Å. Inset scale bar, 5 nm. **e**, Left, SDS–PAGE of N-terminal MBP–VirB4/TrwK fusion purified in the absence of detergents from the cytoplasmic fraction. Right, the negative-stain electron microscopy image of MBP–VirB4/TrwK fusion protein is similar to that of monomeric VirB4/TrwK as shown in **d**. However, an extra MBP density is clearly observable in class averages (inset) and indicates that the VirB4/TrwK N terminus is located in the centre of its long axis. The dimensions of the VirB4/TrwK monomer are compatible with the fitting of six VirB4/TrwK monomers within each IMC barrel. **f**, Western blot against the membrane fraction of a modified $T4SS_{3-10/B4-His6}$ complex purification using anti-His_6 antibody. In the absence of detergent, the membrane fraction was washed iteratively twice with 6 M urea, then once with 0.1 M sodium carbonate pH 11, and finally once with 2 M KCl. Substantial VirB4/TrwK signal remained associated with the membrane fraction after all four stringent washes.

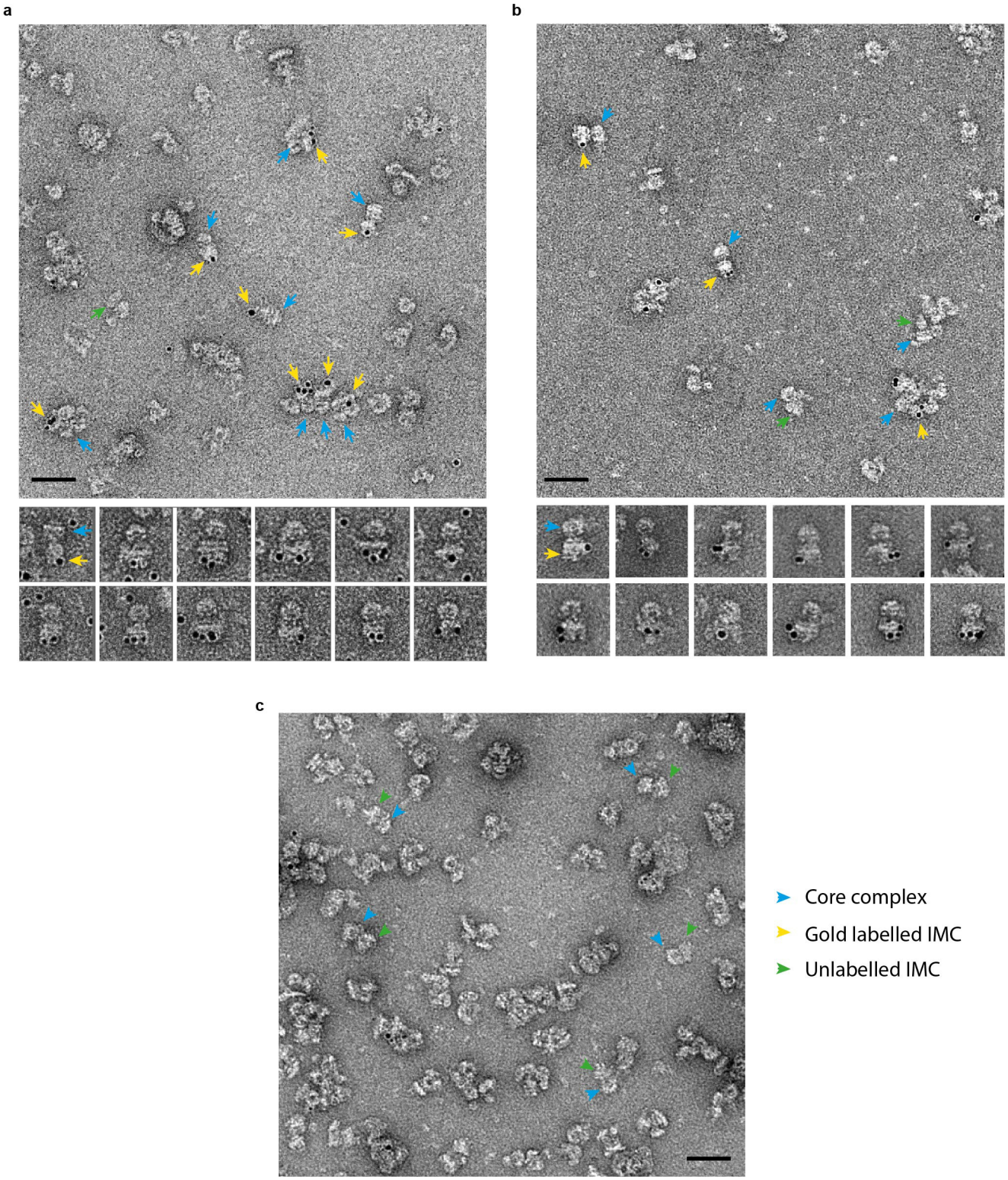

Extended Data Figure 8 | Gold labelling of TrwI/VirB6 and TrwK/VirB4. $T4SS_{3-10}$, $T4SS_{3-10/B4\text{-}His6}$ and $T4SS_{3-10/His6\text{-}B6}$ complexes were purified and applied to carbon-coated grids. His_6 tags were specifically labelled by Ni-NTA nanogold beads (5 nm diameter) directly on the grid before negative staining with 2% uranyl acetate. **a**, Overview and gallery of 12 representative gold-labelled particles of $T4SS_{3-10/B4\text{-}His6}$. **b**, As **a**, but for $T4SS_{3-10/His6\text{-}B6}$. **c**, Overview of the Ni-NTA nanogold bead labelling control experiment using the purified $T4SS_{3-10}$ complex. No gold-labelling was observed. The scale bar in all overview panels is 50 nm.

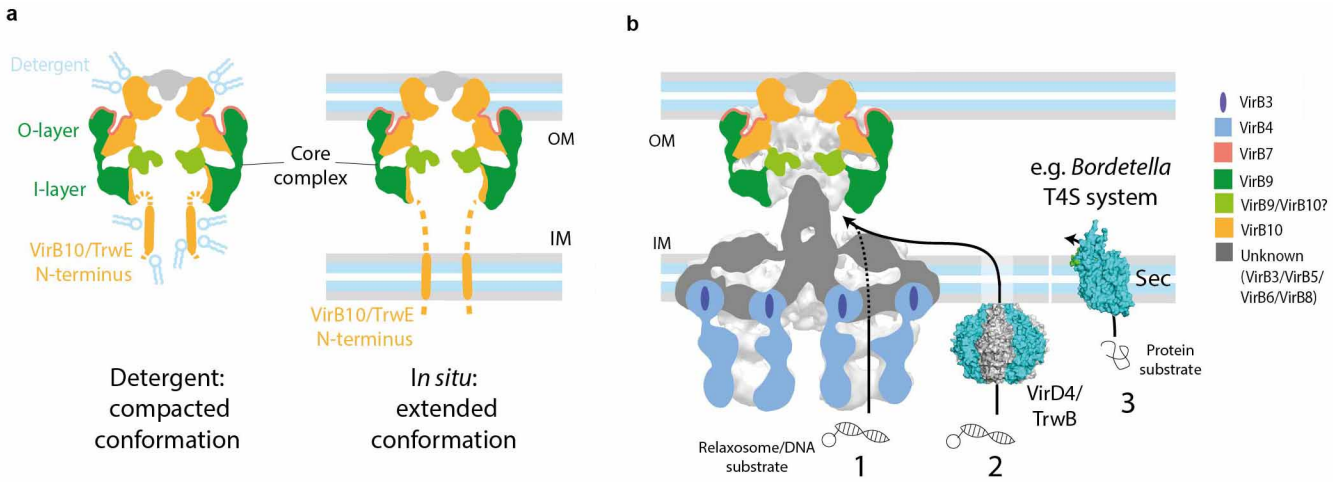

Extended Data Figure 9 | The structure of the T4SS$_{3-10}$ complex is compatible with a general two-step mechanism for T4S systems. a, In earlier studies in which the pKM101 core complex (VirB7/TraN, VirB9/TraO and VirB10/TraF) was purified *in vitro* in isolation[7,10], the flexible N terminus of VirB10/TraF is in an alternate 'compacted' conformation (left) that is positioned immediately under the I-layer to form the core complex 'base'. When the core complex is either *in situ* and is constrained by the inner and outer membranes, or is constrained by other components of the secretion system as observed *in vitro* in the T4SS$_{3-10}$ complex, the VirB10/TrwE N terminus is in an 'extended' conformation (right). The absolute arrangement of the VirB10/TrwE N terminus within the core complex when extended is yet to be determined although the 14 strands may form a rotationally discontinuous punctuated collar that contributes to, or surrounds, the stalk. It should also be noted that we cannot exclude the possibility that, in the membrane environment, the core and inner membrane complexes might be in closer proximity, possibly resulting in the stalk fitting up into the core complex chamber and in VirB10 adopting a less stretched conformation. See **b** for key to colour scheme. **b**, Schematic of the T4SS$_{3-10}$ complex showing three possible entry routes for substrate across the inner membrane and into the core complex inner chamber. In R388 conjugal transfer, the coupling protein VirD4/TrwB probably pumps DNA substrate into the periplasm (route 2), although passage by VirB4/TrwK may currently not be discounted (route 1). Other T4S systems such as that from *Bordetella* use the Sec pathway to transfer effectors across the inner membrane (route 3). For clarity, only VirB nomenclature is used in the colour scheme.

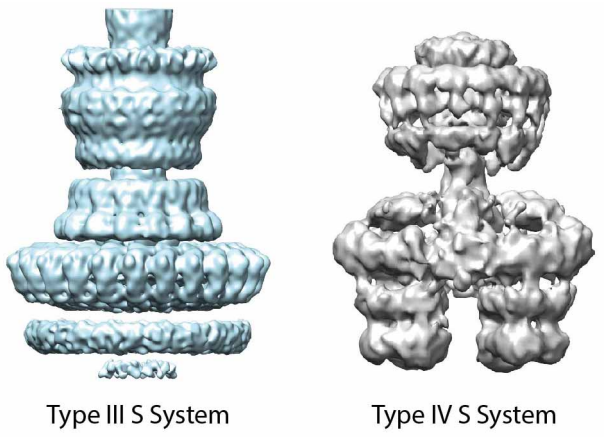

Extended Data Figure 10 | Comparison of the type III and type IV secretion systems. In contrast to the T4S system, the type III secretion (T3S) system (Electron Microscopy Data Bank accession number EMD-1875) has an obvious continuous secretion pore that spans the entire cell envelope, including inner and outer membranes. In addition, the distance between putatively assigned inner and outer membrane locations is slightly extended for the T3S system relative to the T4S system, although this could simply be due to the different systems being derived from different species: *Salmonella* and *Escherichia*, respectively. *In situ*, the T3S system is known to vary in length within the intermembrane space, from 30 to 36 nm (ref. 30).